Emergence of periodic order in electric-field-driven planar nematic liquid crystals: An exclusive ac effect absent in static fields

K. S. Krishnamurthy* and Pramoda Kumar
Centre for Liquid Crystal Research, P.O. Box 1329, Jalahalli, Bangalore 560 013, India
(Received 8 May 2007; revised manuscript received 7 September 2007; published 15 November 2007)

We report, for a nematic liquid crystal with a low conductivity anisotropy, an ac field generated transition from a uniformly planar to a periodically modulated director configuration with the wave vector parallel to the initial director. Significantly, with unblocked electrodes, this instability is not excited by dc fields. Additionally, in very low frequency square wave fields, it occurs transiently after each polarity reversal, vanishing completely during field constancy. The time of occurrence of maximum distortion after polarity reversal decreases exponentially with voltage. The time dependence of optical phase change during transient distortion is nearly Gaussian. The pattern threshold V_c is linear in $\sqrt{f}$, f denoting the frequency; the critical wave number q_c of the modulation scales nearly linearly as $\sqrt{f}$ to a peak at ~50 Hz before falling slightly thereafter. The observed $V_c(f)$ and $q_c(f)$ characteristics differ from the predictions of the standard model (SM). The instability may be interpreted as a special case of the Carr-Helfrich distortion suppressed in static fields due to weak charge focusing and strong charge injection. Its transient nature in the low frequency regime is suggestive of the possible role of gradient flexoelectric effect in its occurrence. The study includes measurement of certain elastic and viscosity parameters relevant to the application of the SM.

DOI: 10.1103/PhysRevE.76.051705 PACS number(s): 61.30.Gd, 47.54.−r, 47.52.+j, 47.20.Lz

I. INTRODUCTION

In nematic monodomains subject to electric fields, bifurcation into patterned states may be driven by different processes [1,2]. The best studied of these is the Carr-Helfrich (CH) mechanism [3]. For planar nematics with the director $\mathbf{n}=(1,0,0)$, in a dc field $\mathbf{E}=(0,0,E)$, the one-dimensional (1D) CH analysis of the coupling between electrical conductivity anisotropy and the bend curvature distortion leads to periodic space charges of alternating sign appearing along the alignment direction x. The body force on these charges sets up periodic cellular flows above a critical voltage V_c determined by the balance between hydrodynamic, dielectric, and elastic torques. The corresponding analysis for an ac field [4] reveals the existence of a cutoff frequency f_c separating two regimes of instability: In the conduction regime, below f_c, the space charges oscillate at the field frequency while the director pattern remains static; beyond f_c, in the dielectric regime, the space charges are static, but the director oscillates. A three-dimensional generalization of the CH theory, referred to as the standard model (SM) [5,6], captures many of the threshold features of anisotropic nematic electroconvection (EC) such as the frequency dependence of the tilt of convective rolls, threshold voltage, and critical wave number of the roll pattern. According to the SM, for an initially planar sample and frequency $f<f_c$, the threshold voltage V_o appropriate to the wave vector $\mathbf{k}=(q,p)$ is given by

$$V_o^2 = \frac{\pi^2 k^*}{\varepsilon_o \varepsilon_a^* - \sigma_a^* \tau \alpha_2 / \eta^*}, \quad \text{with } \tau = \frac{\varepsilon_o \varepsilon_\perp}{\sigma_\perp},$$

$$\varepsilon_a = (\varepsilon_\parallel - \varepsilon_\perp), \quad \sigma_a = (\sigma_\parallel - \sigma_\perp). \tag{1}$$

Here $(^*)$ signifies the effective value of the corresponding material parameter; k, ε_a, σ_a, and η denote, respectively, the elastic modulus, dielectric anisotropy, conductivity anisotropy, and viscosity coefficient; τ is the charge relaxation time and α_2 is a Leslie viscosity coefficient; the subscripts $\parallel$ and $\perp$ specify the directions relative to the initial director. While all the starred quantities involve the components of $\mathbf{k}$, the electrical anisotropies depend additionally on the field frequency. Above a frequency f_L, the so-called Lifshitz point, the threshold pattern consists of normal rolls (NRs) perpendicular to the x axis with the minimum of the neutral curve $V_o(q,p=0)$ occurring at the absolute or critical threshold V_c and wave number q_c; oblique rolls (ORs) form below f_L where $p_c>0$ yields a lower threshold. Beyond f_c, the instability consists of dielectric rolls (DRs) [7] that manifest optically as close-spaced (wavelength, $\lambda <$ sample thickness, d) normal stripes at V_c and as chevronlike oblique stripes above V_c.

Nematics with negative ε_a, positive σ_a, and planar alignment p, referred to conveniently as $(-+p)$ compounds, are established to be ideal candidates for displaying, in the conduction regime, a well ordered sequence of CH instabilities with increasing control parameter, starting with periodic rolls at V_c and developing into chaotic flows far from equilibrium, at ~$2V_c$ [8]. Inspection of Eq. (1) shows that, in such compounds, the CH destabilization is predicted as long as the second term in the denominator offsets the negative first term; and this result is independent of whether the exciting field is static or time varying. In this paper, we provide the first example of a stripes instability resembling the NR state, driven exclusively by ac fields and, contrary to the prediction in Eq. (1), absent in steady fields. In very low frequency fields, it is found to occur only transiently at polarity reversals. We discuss this ac effect in the light of the CH and gradient flexoelectric phenomena.

II. EXPERIMENT

The compound studied is 4-n-pentyloxyphenyl 4-n-decyloxybenzoate (**10/5**), with the

*Corresponding author. murthyksk@gmail.com

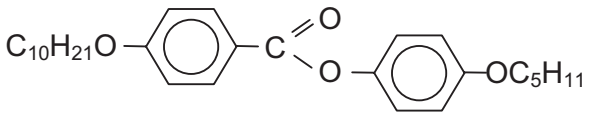

following phase sequence wherein Sm-, *N*, and *I* denote, respectively, the smectic, nematic, and isotropic phases, and T_{AN} and T_{NI} are, respectively, the Sm-*A*–*N* and *N*–*I* transition temperatures:

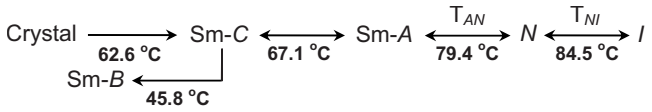

The sample cells were sandwich type, constructed of passivated, indium tin oxide (ITO) coated glass plates from Delta Technologies. The planar alignment was secured through unidirectional rubbing of the cell plates on velvet cloth. The rubbing direction and the layer normal define the reference axes *x* and *z*, respectively. Mylar spacers, heat sealed to the electrodes through cooling from ~250 °C under a uniform pressure, determined the cell gap; cell capacitance was used to measure *d*. Observations were carried out in transmitted light along *z*, using a Leitz DMRXP polarizing microscope, equipped with a Mettler hot stage. The images were recorded using a Sony charge-coupled device camera. The electric field was applied along *z*, employing as the voltage source a Stanford Research Systems DS 345 function generator coupled to a FLC Electronics voltage amplifier (model A800). The applied voltage was measured with a Keithley 2000 multimeter. For measurement of elastic moduli, we carried out both electric and magnetic Freedericksz experiments. Rotational viscosity γ_1 was estimated based on the decay response of the sample from the dielectrically reoriented state [9]. Unless otherwise specified, the following are to be assumed: $(-+p)$ configuration, unblocked electrodes, square wave excitation, $d=30.7$ μm, and sample temperature of 82.6 °C corresponding to the scaled temperature $T^*=(T-T_{NI})/(T_{NI}-T_{AN})=-0.372$.

III. RESULTS AND DISCUSSION

A. Material parameters

For later discussions, we need several electrical, mechanical, and viscosity parameters. We have earlier reported the dielectric and conductivity data for **10/5** [10]; it is useful to note here that the material exhibits σ_a sign inversion close to T_{AN}, at ~81.5 °C, and a variation of σ_a between about −1.2 and 0.4 nS m^{-1} in the nematic range; and it possesses a negative ε_a ranging from −0.35 near T_{AN} to −0.19 near the clearing temperature T_{NI}. At 82.6 °C, the sample temperature mainly used in this study, $\varepsilon_\parallel=3.87$, $\varepsilon_\perp=4.067$, $\sigma_\parallel=5.57$ nS m^{-1}, and $\sigma_\perp=5.36$ nS m^{-1}.

From magnetic Freedericksz experiments, we have determined the temperature dependence of $k_{11}/\Delta\chi$ and $k_{33}/\Delta\chi$, displayed in Fig. 1; here k_{11} and k_{33} are, respectively, the splay and bend elastic moduli, and $\Delta\chi=(\chi_\parallel-\chi_\perp)$ is the diamagnetic anisotropy. Interestingly, as seen in the inset to Fig. 1, $(k_{33}/k_{11})<1$ except close to T_{AN}. Similar anomalous behavior has also been observed in some 4,4′-dialkylazoxybenzenes with long alkyl chains. It is attributed to the flexibility of paraffinic chains leading to banana-shaped molecular conformations and increased effective molecular width [11]. From the ratio k_{33}/k_{11}, and the previously reported data on k_{33} as a function of temperature (based on electric Freedericksz experiments [10]), we arrive at $k_{11}=9.00$ pN and $k_{33}=3.74$ pN at 82.6 °C.

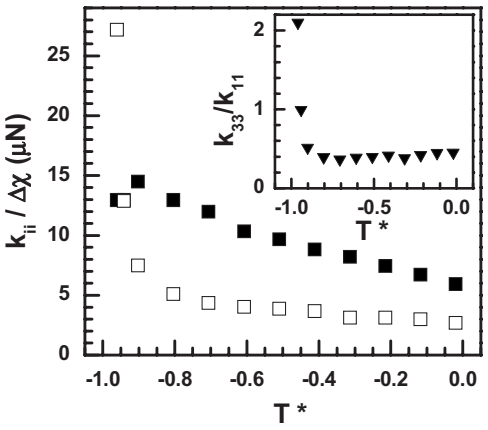

FIG. 1. The ratio of elastic constant k_{ii} to diamagnetic anisotropy $\Delta\chi$ as a function of scaled temperature $T^*=(T-T_{NI})/(T_{AN}-T_{NI})$. Filled squares are for the splay modulus k_{11} and open squares are for the bend modulus k_{33}. The inset shows the unusual temperature dependence of k_{33}/k_{11}.

The Miesovicz viscosities of **10/5** have not been reported. However, η_2 of **10/6** has been measured as a function of temperature [12]; by assuming it to be the same for **10/5** at a given relative temperature, we have $\eta_2=0.0124$ Pa s at $T^*=-0.372$. Further, from the observed scaling properties of the Miesovicz coefficients [13], we may take $(\eta_3/\eta_2)\approx 1.7$ and $(\eta_3/\eta_1)\approx 0.4$. Besides η_i, some of the Leslie coefficients α_i are also relevant to our discussion. To obtain these, we have determined the rotational viscosity γ_1 at various temperatures (Fig. 2); we use the relations $\gamma_1=(\alpha_3-\alpha_2)$, $(\alpha_2+\alpha_3)=(\eta_2-\eta_1)$, and $\alpha_1=2(\eta_1+\eta_2-2\eta_3)-(\alpha_2+\alpha_3)^2/(\alpha_3-\alpha_2)$ to arrive at $\alpha_1=0.0458$ Pa s, $\alpha_2=-0.0418$ Pa s, and $\alpha_3=0.0015$ Pa s.

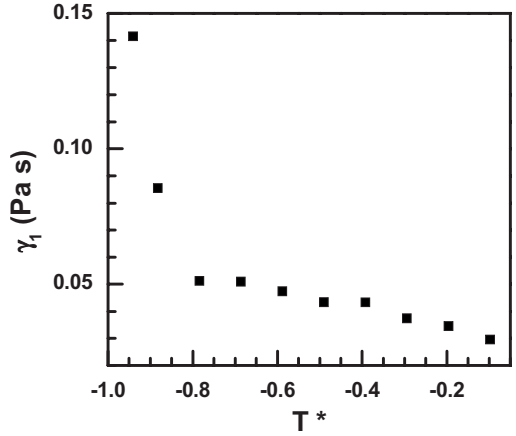

FIG. 2. Temperature dependence of rotational viscosity γ_1 deduced from the decay response of the sample from the dielectrically reoriented state, using capacitance-time measurements.

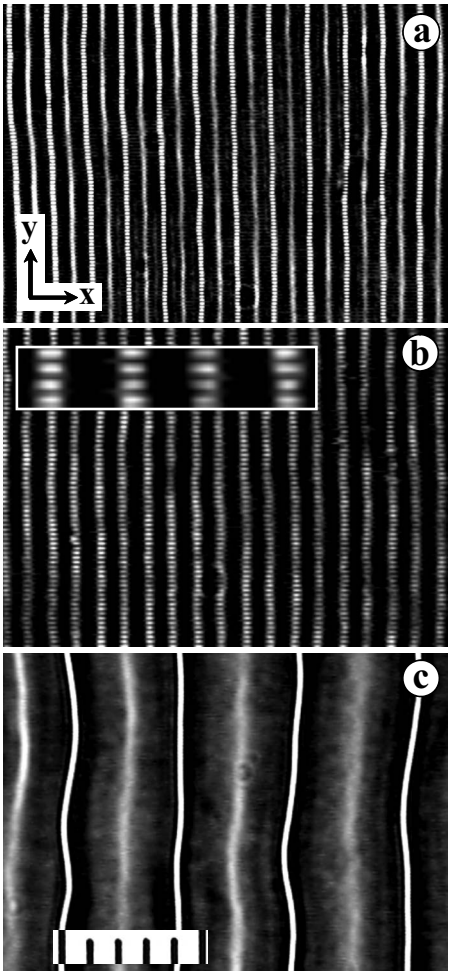

FIG. 3. Striped patterns in a 30.7 μm thick sample of **10/5** at 82.6 °C observed in transmission with the polarizer and analyzer axes parallel to the initial director along x. Bright lines normal to x are the focal images with alternate real images in focus in (a) and (c), and virtual images in focus in (b). For (a) and (b), $f=15$ Hz, $V=24.6$ V; for (c), $f=0.5$ Hz, $V=8$ V. The patterns in (a) and (b) appear steady, but the pattern in (c) appears only during polarity reversals. Each scale division represents 10 μm; the inset in (b) is an enlarged image showing the pairing of virtual lines.

The principal refractive indices n_e and n_o of the sample at $T^*=-0.372$, as determined interferometrically for $\lambda=0.578$ μm (mercury yellow), are 1.5801 and 1.4762, respectively.

B. Field induced deformations

A planar monodomain sample of **10/5**, acted on by a square wave field of fixed frequency $f \geqslant 15$ Hz and progressively increasing voltage amplitude V, bifurcates into a steady pattern of stripes [Figs. 3(a) and 3(b)] above a critical bias V_c; the pattern, which is clearly seen in ordinary light, varies in contrast in linearly polarized light, depending on the vibration direction of the electric vector. When the transmission axis of the polarizer is along x, the visibility is the highest; when it is along y, the pattern practically disappears. Evidently, the stripes are the focal images, analogous to the

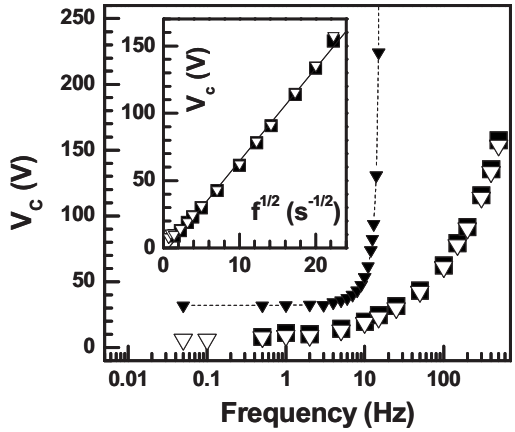

FIG. 4. Threshold voltage V_c at which the periodic order emerges in the originally homogeneous sample, as a function of the field frequency. Below a few Hz, the patterned state occurs transiently after each polarity switch over. Filled squares are for square wave form and open triangles, sine wave form. The inset shows V_c to be linear in $\sqrt{f}$ beyond $f \approx 10$ Hz. The frequency dependence of V_c predicted by the standard model for sine wave driving is indicated by the filled triangles and the dotted line through them. Scaled temperature $T^*=-0.372$.

optical texture of NRs, and are observed due to the modulation of the extraordinary index corresponding to a periodic variation along x of the director tilt θ confined to the xz plane: $\mathbf{n} \approx \mathbf{i} + \mathbf{k}\ \theta_o \cos(2\pi/\lambda)x \cos(\pi/d)z$. In the photomicrograph in Fig. 3(a) for a 15 Hz field, all the bright lines are real images, but they display an alternation in their sharpness as we go from one focal line to the next. This feature is again common to that of the NR optical texture [14], which is explained [15] by considering both the extraordinary wave surface distortion and the deflection of the extraordinary ray from the wave normal. A detailed analysis of the optical field [16,17] based on the Curie principle relating to the symmetry of the director field demonstrates that when light vibrating along x is incident perpendicularly on a nematic layer in the NR state, the emergent nonparallel rays generate an array of cusped caustics; the cusp lines along y, for real caustics, occur alternately on two different z=const planes, with a constant periodicity along x; for virtual caustics, the cusp lines lie in one plane, but their spacing shows double periodicity. Accordingly, in Fig. 3(b), showing the striped pattern recorded under the same conditions as for Fig. 3(a) but with the virtual plane in focus, the line sharpness shows no alternation and also, as the enlarged image in the inset shows, the pairing of the lines, though not conspicuous, is still discernible.

The stripes in **10/5** are predominantly transverse to the initial director in the entire frequency range between ~5 and 600 Hz, the upper f limit having been chosen to keep V_c lower than the dielectric breakdown voltage. Below 5 Hz, the unsteady nature of the patterns does not permit a definitive identification of the stripes as oblique or normal. In Fig. 4, we present the frequency dependence of V_c for both square and sine wave forms. The inset shows the linearity between V_c and $\sqrt{f}$ for frequencies beyond a few Hz. Further, no significant variation in the threshold behavior is seen for the

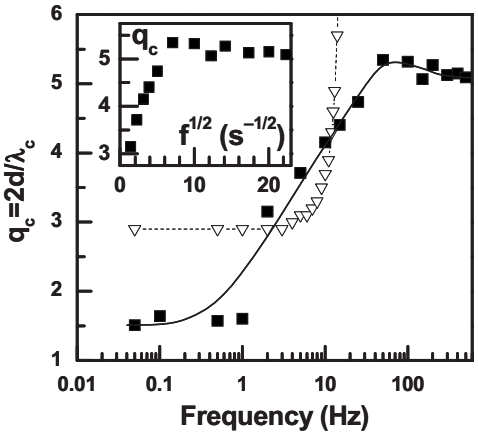

FIG. 5. Critical wave number q_c of the periodic instability due to square wave excitation, in units of π/d, as a function of frequency f (filled squares). The inset shows that the $q_c-\sqrt{f}$ curve is nearly linear for low frequencies and, after rising to a peak value at ~50 Hz, slightly decreases to a saturation value. The frequency dependence of q_c predicted by the standard model for sine wave driving is indicated by the open triangles and the dotted line through them. Scaled temperature $T^*=-0.372$.

two wave forms. Figure 5 depicts the frequency variation of the critical wave number q_c which is nearly linear in $\sqrt{f}$ up to about 50 Hz where a weak maximum occurs; beyond the maximum a slight fall in q_c is indicated.

In the striped pattern state, although field induced motion of dust particles is a common occurrence, this motion is random and does not indicate the presence of coordinated vortical flows such as found in the NR case. However, with increase in V, the pattern turns increasingly time dependent and a quasiturbulent state occurs far from the threshold.

Our central observation that sets the striped patterns in **10/5** apart from the classic NR texture is their transient behavior in the very low frequency regime. For example, the texture in Fig. 3(c) observed for 0.5 Hz appears only during polarity reversals and fades away completely after the field attains constancy. The transmitted intensity profiles in Figs. 6 and 7, which correspond, respectively, to 5 and 15 V of the driving 0.05 Hz square wave field, clearly indicate the momentary occurrence of the instability following each polarity reversal. During each switching, the transmission rises to a peak between two minima, as at M between L and N in Fig. 6, for various voltages up to ~25 V, a feature readily explained by the sample phase difference 2δ. In the field off state, at $T^*=-0.372$, δ_o is, from sample birefringence, $\sim 5.069\pi$, for $\lambda=0.578$ μm and $d=28.2$ μm. In the on state, during the transitory director distortion, the tilt angle θ is a function of x, z, and time t; the excursion of its effective value θ^* between 0 and the maximum $\theta_M{}^*$ results in δ decreasing at first from δ_o to δ_L (L signifying the lowest) and then increasing back to δ_o. For $5\pi > \delta_L > 4.5\pi$, evidently, the transmission profile displays a peak between two equal minima that correspond to 0 normalized intensity and $\delta = 5\pi$. For $4.5\pi > \delta_L > 4\pi$, two equal maxima, corresponding to normalized transmittance $\tau=1$ and $\delta=4.5\pi$, may be expected. We find this doubling of the intensity peak above ~25 V. The inset to Fig. 7 shows two nearly equal well-

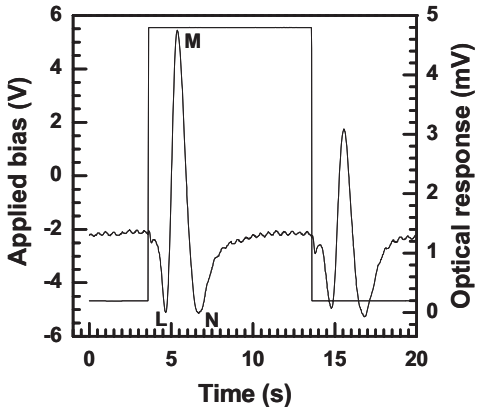

FIG. 6. Electro-optic response in a 28.2 μm thick sample of **10/5** planarly aligned between rubbed, unblocked ITO plates, kept at 82.6 °C, and driven by a 50 mHz, 5 V square wave field. Transient change in transmitted intensity follows each polarity reversal. Diagonally crossed polarizers; incident mercury yellow light.

developed maxima for 30 V, compared to the single maximum for 15 V. The peak optical response of ~37 mV shown in the inset corresponds to $\tau=1$. Thus the τ value to which the initial optical response of ~1.3 mV (Fig. 6) relates is ~0.035 and the corresponding δ_o value of 5.060π is reasonably close to 5.069π obtained using birefringence. In Fig. 8, we present the time dependence of $(\delta_o-\delta_l)$, arrived at using normalized transmittance values, for 5 and 15 V (inset); the solid lines here are the Gaussian fits. With increase in applied bias, the peak transmission occurs increasingly sooner with respect to the time of field reversal. This feature is displayed in Fig. 9.

Besides the transient effects just described for low frequency ac, we find that, in a static field, no patterned instability forms regardless of the voltage and we have verified this by gradually elevating V up to the cell breakdown voltage. This behavior is radically different from that of the usual CH instability which is observed both in ac and dc fields.

In order to determine the sample response to static fields in the dielectrically unstable configuration, we experimented on a homeotropic specimen and found it to undergo the usual

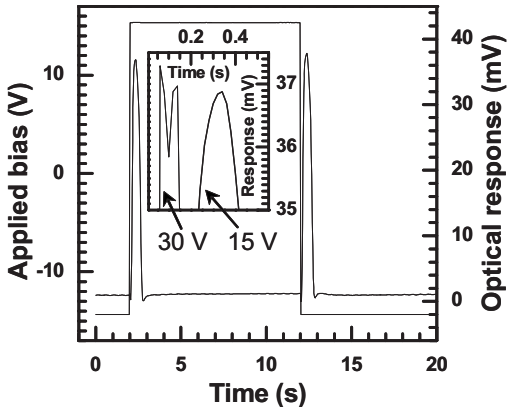

FIG. 7. Electro-optic response in a 28.2 μm thick sample of **10/5** corresponding to 15 V. Other conditions are as in Fig. 6. The inset shows an enlarged view of the first peak for 15 and 30 V.

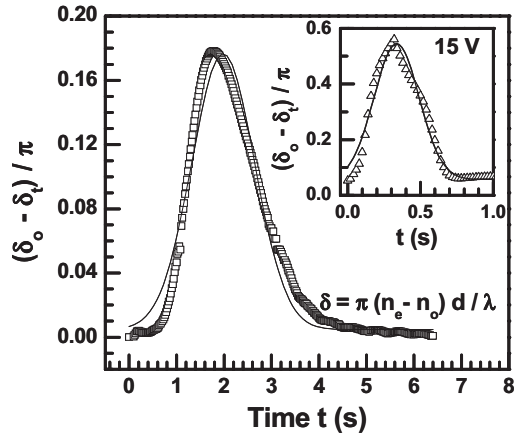

FIG. 8. Relative phase change in units of π as a function of time during the transient occurrence of periodic instability, for 5 and 15 V (inset). The continuous curves are the Gaussian fits.

Freedericksz transition at a threshold V_F; and above V_F the alignment in bulk gradually turns planar. However, again, no dc patterned instabilities occur. In ac fields, as reported in Ref. [10], above some $6V_F$, the reoriented bulk planar region develops the periodic distortion that manifests as normal stripes at threshold and as chevrons at higher voltages and frequencies (>15 Hz); at very high fields, a quasiturbulent situation is reached.

We may now consider the possible role of the CH process in the formation of the patterned state having the characteristics just described. For instance, the normal disposition of the stripes with respect to the unperturbed director may be taken to imply a rather low Lifshitz frequency f_L separating the lower oblique roll (OR) regime from the higher NR regime. In fact, when $\lambda \ll 2d$, $\omega_c = 2\pi f_c$ may be derived from Eq. (1) as [6]

$$\omega_c^2 = \frac{\sigma_\parallel}{\varepsilon_o^2 \varepsilon_\perp}\left[\frac{-\alpha_2}{\eta_1}\left(\frac{\sigma_\parallel}{\varepsilon_\parallel} - \frac{\sigma_a}{\varepsilon_a}\right) - \frac{\sigma_\perp}{\varepsilon_\parallel}\right]. \quad (2)$$

Using the relevant physical parameters mentioned in Sec. III A, f_c is found to be ~16 Hz, and f_L is expected to be only

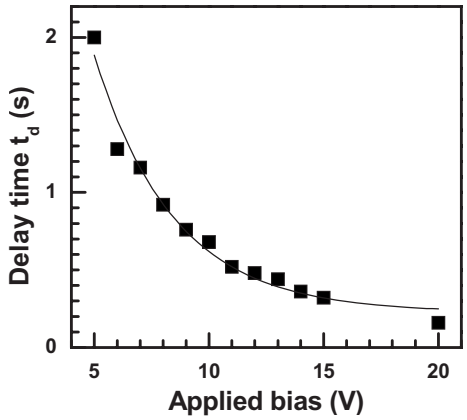

FIG. 9. Voltage variation of switching delay (time of occurrence of peak transmission after polarity reversal) under square wave excitation. The continuous curve is an exponential fit.

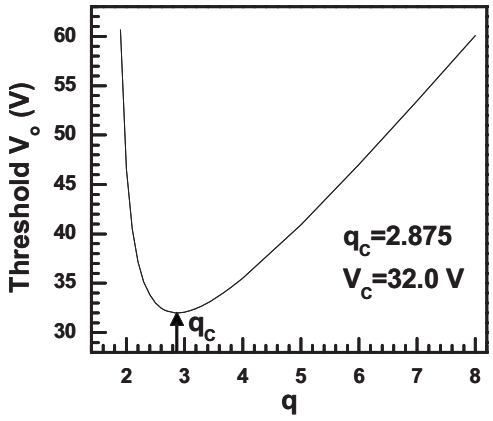

FIG. 10. The neutral curve V_o $(q, p=0)$ for dc excitation and rigid boundary conditions according to the linearized SM.

about $f_c/3$ or 5 Hz [8]. Similarly, the linear increase in V_c with square root of frequency beyond ~15 Hz in Fig. 4 is in accordance with the CH-mechanism based theories applicable to the dielectric regime. In other words, the stripes observed for f>15 Hz may be viewed as the dielectric rolls (DRs). This would also be in consonance with the absence of well coordinated cellular flows in the patterned state formed above ~15 Hz since static vortices are not expected in the dielectric regime [1]. This reasoning is also supported by the frequency dependence of the critical wave number q_c (Fig. 5). We may recall here that the prediction of linearity between bending wave vector and $\sqrt{f}$ neglects the effect of diffusion currents [4]. But q_c cannot indefinitely increase with f since the charge relaxation time gets reduced on the diffusion currents becoming more significant, as would happen when the period of the bending wave is of the order of the Debye-Hückel screening length. As a consequence, the $q_c - \sqrt{f}$ plot may be expected to display a maximum in the dielectric regime [18].

If the foregoing interpretation of the patterned state beyond f_c is valid, how do we understand the absence of electrohydrodynamic (EH) states in the conduction regime under dc excitation? In fact, Eq. (1) gives the dc neutral curve V_o $(q,p=0)$ shown in Fig. 10, indicating 32.0 V as the critical voltage corresponding to the critical wave number of ~2.87 [19]. At this high voltage, the reduction of the bulk field due to the formation of double layers at the electrodes is likely to be negligible [20]. Despite these facts, the CH charge focusing is ineffective under dc driving and an obvious cause for this could be the charge injection. To be definitive, the patterned instability is due to the CH term, $[(\alpha_3/q^2)-\alpha_2]\tau_q\sigma_a^*$ [21] which works out to be ~0.13 N μs^2 S/m^3 for **10/5** corresponding to the q_c value in Fig. 7; by comparison, its value is ~2.29 N μs^2 S/m^3 for the room-temperature nematic methoxybenzylidene butylaniline, MBBA, with the data from Ref. [5]. Thus it is conceivable that the weak charge focusing effect in **10/5** is disrupted by the unipolar charge injection present for static or very low frequency fields. In order to experimentally test this idea, we studied the instabilities using cells constructed of polyimide-coated ITO plates. In this case, under dc driving, the usual Williams striations are observed above a critical voltage V_{dc} (Fig. 11).

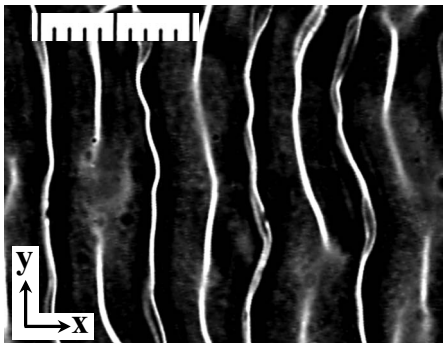

FIG. 11. Pattern of oblique rolls observed in a 51 μm thick sample of **10/5**, planarly aligned between polyimide coated and rubbed ITO plates, kept between parallel polarizers along x at 82.6 °C, and driven by a dc field corresponding to 18.3 V $\approx 1.4V_c$. The rolls are oscillatory as well as traveling. Real line images are in focus.

In low frequency fields, the same texture appears above V_{dc} during intervals of field constancy and it is transiently perturbed during polarity switch over. Further, even below V_{dc}, the stripes form transiently at polarity reversals.

The transient occurrence of the periodic order at field polarity switchings is suggestive of a possible role of flexoelectric response in its origin. The effective molecular field $\mathbf{h}$ which determines the flexoelectric torque $\mathbf{\Gamma}_F = \mathbf{n} \times \mathbf{h}$ is expressible as [22] $\mathbf{h} = (e_1 - e_3)(\mathbf{E}\nabla \cdot \mathbf{E} - \nabla \mathbf{n} \cdot \mathbf{E}) - (e_1 + e_3)\mathbf{n} \cdot \nabla \mathbf{E}$ where e_1 and e_3 are the splay and bend flexocoefficients, respectively. The volume torque due to the coupling of dipolar flexopolarization with the applied field involves $(e_1 - e_3)$ and that of quadrupole density with the field gradient $(e_1 + e_3)$. Influence of flexoeffect on nematic electroconvection has been analyzed within both the 1D and 3D descriptions [23], considering, besides the $(e_1 - e_3)$ terms, the $(e_1 + e_3)$ terms due to the transverse field gradients. Broadly, the results indicate for the dc case a lowering of the threshold and bifurcation into the oblique rather than normal roll state at the onset for MBBA. In no situation, the stability of the rest state under a constant field is predicted.

We may now consider the possible existence of a field gradient along z. For an applied dc voltage, the equilibrium field distribution in a weakly conducting nematic is necessarily inhomogeneous, but this may not apply to the bulk. For instance, with blocking layers preventing charge injection, voltage induced diffuse counterion layers formed next to the electrodes so modify the field that it is usually homogeneous in bulk and rapidly increasing toward the electrodes in the Debye-like screening layers [20]. Additionally, when selective adsorption of ions of the same sign occurs at these layers, permanent surface field asymmetry may result; differential mobility of the opposite charge carriers also produces a similar field change, except that the surface field asymmetry is now transient [24]. When no blocking layers are applied to the electrodes, in a rather thick sample (1 cm), charge injection has been demonstrated to render the surface field asymmetric while leaving the bulk field uniform [25]. Thus the bulk field inhomogeneity leading to a volume flexoeffect may normally be expected only transiently following polarity reversals. This effect may be particularly pronounced in the presence of intrinsic double layers formed due to selective ion absorption as discussed by us in [26].

Notwithstanding the aforesaid results on field constancy in bulk, there are also reports to the contrary in thin films [27–29]. For instance, under dc excitation, Derzhanski *et al.* [27] consider it probable to have a linear field gradient in thin samples and a hyperbolic gradient in thick ones. Thus they interpret the experimental electrooptic behavior in some nematics relating to nonpatterned and longitudinal periodic distortion states as of gradient flexoelectric origin. Further, as Derzhanski and Petrov have shown [28], a gradient flexoelectric (GF) effect may modify the threshold features of the longitudinal domain instability in the Bobylev-Pikin and Pikin-Indenbom regimes. Furthermore, thin planar samples, which are dielectrically stable and nonelectroconvecting, may display a GF volume instability that mimics the homogeneous splay-Freedericksz distortion. For definiteness, if we take the field distribution to be linear, given by

$$E(z) = \frac{E_a + E_c}{2} - \frac{z(E_a - E_c)}{d}, \tag{3}$$

where E_a denotes the anode field at $z = -d/2$ and E_c, the cathode field at $z = +d/2$, and the local director $\mathbf{n} = \mathbf{i} \cos\theta + \mathbf{k} \sin\theta$, then the GF torque is $\mathbf{\Gamma}_{GF} = \mathbf{j}\,(e_1 + e_3) \cos\theta \sin\theta\, (E_a - E_c)/d$. Depending on the sign of the total flexocoefficient, $\mathbf{\Gamma}_{GF}$ could exercise either a stabilizing or destabilizing effect on the planar state. In the latter case, a balance between the elastic and GF torques determines the threshold for the GF analog of the dielectric instability.

The foregoing results suggest two alternative interpretations of the transient patterning behavior in **10/5**, both involving the GF response. First, if under steady field conditions the bulk field is assumed to be homogeneous, $\mathbf{\Gamma}_{GF}$ would be 0 and the absence of instability would imply a disruptive influence of the charge injection on the CH charge focusing process. However, consequent on polarity change, as argued in [26], field gradients that come to exist momentarily may generate a nonzero torque $\mathbf{\Gamma}_{GF}$. If the sign of $\mathbf{\Gamma}_{GF}$ is such as to destabilize the planar state and support the CH process, bifurcation to the periodic state could occur. In all likelihood, the period selection is by the principle of fastest growing CH mode. Alternatively, if the bulk field gradient is assumed to exist in the steady field condition, by implication, $\mathbf{\Gamma}_{GF}$ would be stabilizing and suppressive of the CH process to prevent any pattern formation. During and briefly after the field polarity change over, conditions suitable for $\mathbf{\Gamma}_{GF}$ to be of the right sign to transiently augment the CH destabilizing torque could develop to result in the periodic order. Obviously the sign of the total flexocoefficient is crucial for the choice between these two possibilities.

We note here that the charging process in itself occupies a very short time, less than a millisecond. But the time for charge drift τ_d across the cell due to polarity change over may take a few seconds. Under steady ion transport, $\tau_d = (6\pi\eta r/e)(d^2/V)$ where η is the effective viscosity, r is the ionic radius, and e is the elementary charge. For argument, we may take the ion, to which a few of the surrounding

mesogenic molecules may attach themselves by virtue of their polar nature, to have an effective radius of ~5 nm; further, taking $\eta=0.05$ Pa s, we obtain $\tau_d \approx 4.8$ s for a 28.2 μm thick sample subject to 5 V as for Fig. 6. In this interval, field-gradient variations necessary for the transient GF instability may be obtained. Correspondingly, the transmitted light intensity variation due to this instability may last for a few seconds as in Fig. 6.

Before concluding, we may recall that there have been earlier investigations on electric field effects in several homologs belonging to the series 4-n-alkoxyphenyl-4-n′-alkoxybenzoates other than **10/5** [30–33]. These studies deal with the instabilities driven by sine wave fields of not too low a frequency and make no mention of the type of transient pattern formation encountered here. More specifically, Brand *et al.* [31] observe in **10/6** a 1D pattern of normal rolls at the onset in the high T^* region of positive σ_a; and a 2D pattern of short normal rolls, in the intermediate T^* region wherein σ_a remains positive. Assuming the viscosity coefficients of 4-n-octyl-4′-cyanobiphenyl for **10/6**, they attribute the pattern variation to the sign of α_3 which changes from negative to positive between the two T^* regions. They also find the experimental values of V_c and q_c to be lower than the values predicted by the SM by at least a factor of 2. However, this conclusion is not supported by subsequent investigations on **10/6** [32] in which the measured value of $|\varepsilon_a|$ for the material is found to be much lower than that reported in [31]. In fact, in [32], planar samples driven by ac fields are observed, in the high temperature regime of positive σ_a, to exhibit a normal electroconvective behavior; here, the SM predictions are arrived at by choosing the elastic and viscosity parameters so as to obtain the best fits for $V_c(f)$ and $\mathbf{k}(f)$. Similarly, in a more recent report [33], the pattern characteristics for **8/7** at $T^*=-0.1$ are found to match very well with those of standard $(-+p)$ nematics.

Now we may compare the aforesaid results for **10/6** with ours for **10/5**; we find, at $T^*=-0.372$ at which both σ_a and α_3 are positive, a 1D normal stripes pattern instead of a rectangular pattern reported in [31] for $\sigma_a>0$ and $\alpha_3>0$. The predicted $V_c(f)$ and $q_c(f)$ plots for **10/5**, determined from Eq. (1), are presented in Figs. 4 and 5; the calculated V_c strongly diverges around 15 Hz, being some 900 V at 16 Hz; it is about five times the observed threshold around 1 Hz and 2.8 times, at 10 Hz. Corresponding variations are also seen for q_c in Fig. 5. These features may seem anomalous when one considers the reported conformity of the experimental $V_c(f)$ and $q_c(f)$ data to the SM in **10/6** with $V_c \approx 10$ V and $q_c \approx 1.6$ in the low frequency limit, at $T^*=-0.2$ [32], compared to $V_c=32$ V and $q_c \approx 2.9$ in Fig. 10. It should, however, be noted that, at the scaled temperature considered $(=-0.372)$, the value of $(\sigma_a/\sigma_\perp)$ for **10/6** [32] is almost four times that for **10/5**; also k_{33}/k_{11} required for the best fit in [32] is ~1.3 whereas its measured value in **10/5** is only ~0.42. These differences together with, to a lesser extent, the changes in the value of other material parameters, could explain the apparent anomaly mentioned. It is also significant that in [32] both oblique rolls $(p \neq 0, f<f_L)$ and normal rolls $(p=0, f>f_L)$ are considered whereas our calculations are limited only to the normal roll case.

IV. CONCLUSIONS

In so far as electroconvection due to conductivity anisotropy in $(-+p)$ nematics is concerned, from earlier reports, no essential distinction between static and low frequency ac excitations has been known to exist, either theoretically or experimentally. Here we have demonstrated that, for a nematic in which the CH destabilization term is relatively small and charge injection is not blocked, the low frequency striped pattern generated in ac is completely absent in dc. Additionally, under very low frequency driving, the pattern state develops only transitorily after each polarity switching. These differences for ac and dc fields do not exist when charge injection is suppressed with polyimide blocked electrodes. The question as to how exactly the charge injection could prevent the CH destabilization remains open. Similarly the patterned instability, observed during unsteady conditions of ion transit across the sample under very low frequency ac driving, needs a closer examination to determine the role of GF effect in its origin.

ACKNOWLEDGMENTS

We thank Professor K. A. Suresh for his keen interest in this investigation, Dr. S. Krishna Prasad and Professor W. Weissflog for the liquid crystal samples, and Professor A. G. Petrov for useful suggestions relating to gradient flexoinfluence. P.K. acknowledges support from the Council of Scientific and Industrial Research, India.

[1] L. M. Blinov and V. G. Chigrinov, *Electrooptic Effects in Liquid Crystal Materials* (Springer, Berlin, 1994), Chap. 4.
[2] S. A. Pikin, *Structural Transformations in Liquid Crystals* (Gordon and Breach Science Publishers, New York, 1991).
[3] W. Helfrich, J. Chem. Phys. **51**, 4092 (1969).
[4] E. Dubois-Violette, P. G. de Gennes, and O. Parodi, J. Phys. (Paris) **32**, 305 (1971).
[5] E. Bodenschatz, W. Zimmermann, and L. Kramer, J. Phys. (Paris) **49**, 1875 (1988).
[6] L. Kramer and W. Pesch, in *Pattern Formation in Liquid Crystals*, edited by A. Buka and L. Kramer (Springer, Berlin, 1996), Chap. 6.
[7] M. Scheuring, L. Kramer, and J. Peinke, Phys. Rev. E **58**, 2018 (1998).
[8] R. Ribotta, in *Solitons in Liquid Crystals*, edited by L. Lam and J. Prost (Springer, Berlin, 1992).
[9] H. Wang, T. X. Wu, X. Zhu, and Shin-Tson Wu, J. Appl. Phys. **95**, 5502 (2004).
[10] P. Kumar, S. N. Patil, U. S. Hiremath, and K. S. Krishnamurthy, J. Phys. Chem. **111**, 8792 (2007).
[11] W. H. de Jeu and W. A. P. Claassen, J. Chem. Phys. **67**, 3705 (1977).

[12] D. Demus, M. Pohl, S. Schönberg, L. Weber, A. Wiegeleben, and Weißflog, in *Forschungen über flüssige Kristalle*, edited by D. Demus (Martin-Luther-Universatät Halle-Winttenberg, Halle, 1983), p. 18.
[13] M. Simoes, S. M. Domiciano, and F. S. Alves, Liq. Cryst. **33**, 849 (2006).
[14] P. A. Penz, Mol. Cryst. Liq. Cryst. **15**, 141 (1971).
[15] K. Kondo, A. Fukuda, and E. Kuze, Jpn. J. Appl. Phys. **20**, 1779 (1981).
[16] A. Joets, A. Belaidi, and R. Ribotta, in *Geometry and Topology of Caustics-Caustics 2002* (Banach Centre Pub. 62, Warsaw, 2004).
[17] E. Plaut, A. Joets, and R. Ribotta, J. Phys. III **7**, 2459 (1997).
[18] Y. Galerne, G. Durand, and M. Veyssie, Phys. Rev. A **6**, 484 (1972).
[19] The effective material parameters in Eq. (1), for $p=0$, are given by [6] $k^*=k_{11}+k_{33}q^2$, $\varepsilon_a^*=\varepsilon_a(1+q^2)$ $(\Sigma^{-1}+\omega'^2D^{-1})/(1+\omega'^2)$, $\sigma_a^*=\sigma_a[(D/\Sigma)-(\varepsilon_a\sigma_\perp)/(\varepsilon_\perp\sigma_a)]/(1+\omega'^2)$, and $\eta^* \approx \eta_1+(\eta_1+\eta_2+\alpha_1)/q^2$, with $\Sigma=1+\omega^2(\sigma_\parallel/\sigma_\perp)$, $D=1+q^2(\varepsilon_\parallel/\varepsilon_\perp)$, $\omega'=\omega\tau_q D/\Sigma$, and the wave vector q in units of π/d.
[20] G. Barbero, D. Olivero, N. Scaramuzza, G. Strangi, and C. Versace, Phys. Rev. E **69**, 021713 (2004).
[21] A. Buka, N. Eber, W. Pesch, and L. Kramer, in *Self Assembly, Pattern Formation and Growth Phenomenon in Nano-Systems*, edited by A. A. Golovin and A. A. Nepomnyashchy (Springer, Berlin, 2006). It is to be noted that, in Eq. (1), $[(\alpha_3/q^2)-\alpha_2]\tau_q\sigma_a^*$ is approximated to the second term in view of the relatively very low value of the first term.
[22] A. G. Petrov, in *Physical Properties of Liquid Crystals: Nematics*, edited by D. A. Dunmur, A. Fukuda, and G. R. Luckhurst (INSPEC-IEE, London, 2001), p. 251.
[23] N. V. Madhusudana and V. A. Raghunathan, Liq. Cryst. **5**, 1789 (1989); L. Kramer, E. Bodenschatz, W. Pesch, W. Thom, and W. Zimmermann, *ibid.* **5**, 699 (1989).
[24] R. N. Thurston, J. Cheng, R. B. Meyer, and G. D. Boyd, J. Appl. Phys. **56**, 263 (1984).
[25] Sun Lu and D. Jones, Appl. Phys. Lett. **16**, 484 (1970).
[26] P. Kumar and K. S. Krishnamurthy, Liq. Cryst. **34**, 257 (2007).
[27] A. I. Derzhanski, A. G. Petrov, H. P. Hinov, and B. L. Markovski, Bulg. J. Phys. **1**, 165 (1974).
[28] A. I. Derzhanski and A. G. Petrov, Acta Phys. Pol. A **55**, 747 (1979).
[29] A. Derzhanski and A. G. Petrov, in *Advances in Liquid Crystal Research and Applications*, edited by L. Bata (Pergamon Press, Oxford, 1980), Vol. 1, p. 515.
[30] M. Petrov, and P. Simova, in *Forschungen über flüssige Kristalle*, edited by D. Demus (Martin-Luther-Universatät Halle-Winttenberg, Halle, 1983), p. 72.
[31] H. R. Brand, C. Fradin, P. L. Finn, W. Pesch, and P. E. Cladis, Phys. Lett. A **235**, 508 (1998).
[32] E. Kochowska, S. Nemeth, G. Pelzl, and A. Buka, Phys. Rev. E **70**, 011711 (2004).
[33] T. Toth-Katona, A. Cauquil-Vergnes, N. Eber, and A. Buka, Phys. Rev. E **75**, 066210 (2007).